J Biomol NMR (2015) 63:375–388
DOI 10.1007/s10858-015-9997-5

ARTICLE

Proton detection for signal enhancement in solid-state NMR experiments on mobile species in membrane proteins

Meaghan E. Ward[1,2] · Emily Ritz[1,2] · Mumdooh A. M. Ahmed[1,2,3,4] · Vladimir V. Bamm[2,3] · George Harauz[2,3] · Leonid S. Brown[1,2] · Vladimir Ladizhansky[1,2]

Received: 2 September 2015 / Accepted: 15 October 2015 / Published online: 22 October 2015

Abstract Direct proton detection is becoming an increasingly popular method for enhancing sensitivity in solid-state nuclear magnetic resonance spectroscopy. Generally, these experiments require extensive deuteration of the protein, fast magic angle spinning (MAS), or a combination of both. Here, we implement direct proton detection to selectively observe the mobile entities in fully-protonated membrane proteins at moderate MAS frequencies. We demonstrate this method on two proteins that exhibit different motional regimes. Myelin basic protein is an intrinsically-disordered, peripherally membrane-associated protein that is highly flexible, whereas *Anabaena* sensory rhodopsin is composed of seven rigid transmembrane α-helices connected by mobile loop regions. In both cases, we observe narrow proton linewidths and, on average, a 10× increase in sensitivity in 2D insensitive nuclear enhancement of polarization transfer-based HSQC experiments when proton detection is compared to carbon detection. We further show that our proton-detected experiments can be easily extended to three dimensions and used to build complete amino acid systems, including sidechain protons, and obtain inter-residue correlations. Additionally, we detect signals which do not correspond to amino acids, but rather to lipids and/or carbohydrates which interact strongly with membrane proteins.

Keywords Membrane proteins · Solid-state nuclear magnetic resonance (SSNMR) · Magic angle spinning (MAS) · Proton detection · J-couplings · INEPT

Introduction

Solid-state nuclear magnetic resonance (SSNMR) spectroscopy is an emerging method which can be utilized to obtain high-resolution structural and dynamical information on crystalline, membrane-associated, and fibrillar proteins. As molecular tumbling is suppressed in such samples, their NMR spectra are broadened by strong anisotropic interactions. Most commonly, magic angle spinning (MAS) (Andrew et al. 1958; Lowe 1959) in combination with high power decoupling (Mehring et al. 1971) is utilized to average out these interactions and to re-establish high resolution for low gamma nuclei such as ^{13}C or ^{15}N. In contrast, the linewidths of protons remain prohibitively broad at moderate MAS frequencies (10–20 kHz) due to the strong inter-proton dipolar couplings.

The implementation of proton detection provides an increase in sensitivity, additional chemical shift data, and more sensitive probes of conformational and environmental changes (Mulder et al. 2000; Weiningner et al. 2013). Recent advances in high magnetic field and fast MAS probe technologies (Parthasarathy et al. 2013; Kobayashi et al. 2013; Ye et al. 2014; Nishiyama et al. 2014; Agarwal et al. 2014) and sample preparation protocols (McDermott

Electronic supplementary material The online version of this article (doi:10.1007/s10858-015-9997-5) contains supplementary material, which is available to authorized users.

✉ Vladimir Ladizhansky
vladizha@uoguelph.ca

[1] Department of Physics, University of Guelph, Guelph, ON, Canada

[2] Biophysics Interdepartmental Group, University of Guelph, Guelph, ON, Canada

[3] Department of Molecular and Cellular Biology, University of Guelph, Guelph, ON, Canada

[4] Present Address: The Department of Physics, Faculty of Science, Suez University, Suez 43533, Egypt

et al. 1992; Reif et al. 2001; Paulson et al. 2003; Chevelkov et al. 2003) have enabled the use of proton detection in many systems with limited mobility. Through the use of dipolar-based correlation experiments, linewidths of ~0.2 ppm (160–180 Hz at 800 MHz field strength) could be achieved on fully-protonated samples at MAS rates of 40–60 kHz (Zhou et al. 2007; Marchetti et al. 2012; Lamley et al. 2014; Weingarth et al. 2014; Agarwal et al. 2014; Dannatt et al. 2015), and could be significantly improved by combining high spinning frequencies with perdeuteration of the sample and the re-introduction of protons at exchangeable sites through back-exchange with protonated buffer (Reif et al. 2006; Chevelkov et al. 2006; Agarwal and Reif 2008; Asami et al. 2010; Linser et al. 2011; Ward et al. 2011; Chevelkov et al. 2014; Barbet-Massin et al. 2014; Agarwal et al. 2014).

Although the perdeuteration of proteins is necessary to achieve sufficiently narrow proton linewidths, this method is limiting as only exchangeable protons, such as amide protons and exchangeable sidechain protons, are detectable. Thus, SSNMR experiments on fully-deuterated samples are restricted to those which specifically detect these atoms, and sidechain proton assignments are difficult to obtain. To combat this deficiency, additional protons can be sparsely incorporated into the sample at low levels through the reduced adjoining protonation (RAP) labeling scheme (Asami et al. 2010) or the selective reintroduction of protons into methyl-bearing sidechains (Goto and Kay 2000; Agarwal et al. 2006, 2008; Huber et al. 2011) without major sacrifices to the linewidth.

Proton–proton dipolar interactions are averaged not only by MAS, but also by local motions. For example, resolution approaching that obtained in solution NMR samples can be observed in high resolution (HR)-MAS spectra. In these experiments non-solid materials, such as tissue samples and swollen resins, are spun about the magic angle at low frequencies (~2–5 kHz) which, due to the high mobility of the samples, is sufficient to completely average the dipolar couplings (Anderson et al. 1995; Keifer et al. 1996; Maas et al. 1996; Cheng et al. 1996).

Typically, structured proteins consist of rigid secondary structural elements which are linked by more flexible, and often less structured, loops and turns. Within these less structured regions, local, sub-microsecond molecular motions of sufficiently large amplitude can lead to an averaging of the dipolar interaction. This can result in a reduction of the linewidths, but also often leads to reduced sensitivity for these residues in the dipolar-based two- and three-dimensional chemical shift correlation experiments which are used to study the well-structured regions of proteins. However, the averaging of the strong dipolar interactions facilitates through-bond polarization transfers, which are based on the comparatively weak J-interaction. Thus, through the utilization of polarization transfer methods such as insensitive nuclear enhancement of polarization transfer (INEPT) (Morris and Freeman 1979), the mobile regions of a protein can be selectively excited (Chen et al. 2007; Tian et al. 2009) and excellent resolution can be obtained indirectly in the proton dimension, even without the use of extensive deuteration or fast MAS. This has been demonstrated previously on the mobile regions of integral and peripheral membrane proteins (Andronesi et al. 2005; Etzkorn et al. 2007; Zhong et al. 2007; Yang et al. 2011), histones (Gao et al. 2013), and amyloid fibrils (Helmus et al. 2010; Van Melckebeke et al. 2011).

Here, we establish the utility of high-sensitivity direct proton detection of mobile fragments in fully-protonated proteins at moderate spinning frequencies. INEPT-based experiments were carried out on two proteins which exhibit very different motional regimes. The first of the two, myelin basic protein (MBP, 18.5-kDa splice isoform), depicted in Fig. 1a, belongs to the class of intrinsically-disordered proteins. As a major component of the myelin sheath in the brain and spinal cord, the primary function of MBP is believed to be maintenance of the compaction of the myelin sheath through association with the cytoplasmic faces of the oligodendrocyte membrane (Hu et al. 2004; Min et al. 2009; Harauz and Boggs 2013). In doing so, MBP peripherally interacts with lipid membranes, forming three surface-seeking amphipathic α-helices (Bates et al. 2003; Harauz et al. 2009) which are linked by highly flexible, unstructured regions (Zhong et al. 2007). MBP has also been demonstrated to associate with many other

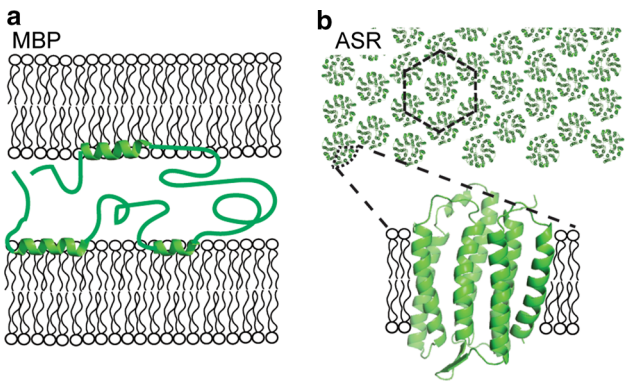

Fig. 1 **a** Schematic representation of 18.5-kDa MBP. Upon interaction with lipids, MBP forms three short amphipathic α-helices, whereas the majority of the protein remains unstructured. The arrangement shown represents one of many possible arrangements of MBP in the compact myelin environment, as the mechanisms through which MBP-lipid interactions across apposing membrane leaflets occur are unknown. **b** Schematic representation of lipid reconstituted ASR. In our SSNMR samples, ASR has been shown to form a hexagonal lattice of trimers. The majority of the protein is tightly structured as an intramembrane α-helical bundle, although the loop regions which join these helices may experience significant motions

proteins, gaining partial secondary structure upon these interactions as well (Polverini et al. 2008; Ahmed et al. 2009; Harauz and Libich 2009; Libich et al. 2010; Ahmed et al. 2012; De Avila et al. 2014). Previous SSNMR studies of MBP in a myelin-mimetic lipid environment have shown that the unstructured or extended regions can be observed by ^{13}C-detected INEPT-based spectroscopy with typical proton linewidths of 0.15–0.2 ppm at 600 MHz field strength (Zhong et al. 2007), whereas one of the less mobile peripheral α-helices, the immunodominant epitope comprising residues N81–S99, exhibited proton line widths on the order of 0.3–0.7 ppm at 800 MHz field strength and has been observed through dipolar-based correlation spectroscopy (Ahmed et al. 2010).

The second example, a seven transmembrane (TM) α-helical protein, *Anabaena* sensory rhodopsin (ASR) (Jung et al. 2003), depicted in Fig. 1b, is largely composed of rigid TM α-helices which are joined by less structured, shorter loop regions and has been found to form a hexagonal lattice of trimers in our samples (Wang et al. 2012; Ward et al. 2015). Solid-state NMR resonance assignments for approximately 90 % of ASR's residues have been obtained using through-space polarization transfer techniques (Shi et al. 2011; Wang et al. 2013b), and a high resolution trimer structure has been calculated from internuclear distances, torsional restraints, and paramagnetic relaxation enhancements (Wang et al. 2012, 2013a). Despite the increased mobility in some of the loop regions, many of these residues can be observed in dipolar-based experiments, although frequently with lower sensitivity (Good et al. 2014), indicating that the motions in these loops are much more restricted than those present in the unstructured regions of MBP.

Through the use of INEPT-based spectroscopy, we can selectively observe many protein resonances with intrinsically narrow linewidths in both ASR and MBP. In addition to protein resonances, we observe several peaks in the ASR spectra which likely correspond to isotopically-labeled lipids or carbohydrates which originate from the *E. coli* membranes, co-purify with the protein, and are tightly bound to it. With the implementation of direct proton detection, sensitivity enhancements of up to tenfold can be achieved for the observed regions of both MBP and ASR in two-dimensional ^{1}H–^{13}C INEPT HSQC experiments. To further study the mobile regions of MBP and ASR, this two-dimensional proton-detected experiment was extended to three dimensions through the incorporation of proton–proton mixing. In MBP, this step facilitates the detection of sidechain protons, and the determination of inter-residue correlations. In ASR, proton chemical shifts can be added to many of the spin systems corresponding to the mobile fragments of molecules which interact strongly with the protein.

Materials and methods

Materials

Common chemicals of reagent grade were purchased from either Fisher Scientific (Unionville, ON, Canada) or Sigma-Aldrich (Oakville, ON, Canada). Isotopically-labeled compounds, such as $^{15}NH_4Cl$ and $^{13}C_6$-glucose, were obtained from Sigma-Aldrich or Cambridge Isotope Laboratories (CIL, Andover, MA, USA). The Ni^{2+}-NTA (nitrilotriacetic acid) agarose resin was purchased from Qiagen (Mississauga, Ontario, Canada). Lipids were purchased from Avanti Polar Lipids (Alabaster, AL, USA).

Sample preparation

Expression, purification, and reconstitution of myelin basic protein

Uniformly ^{13}C- and ^{15}N-labeled wild-type, 18.5-kDa recombinant murine myelin basic protein (UCN MBP) was expressed in *E. coli* BL21-CodonPlus(DE3)-RP cells (Stratagene, La Jolla, CA, USA) and purified by nickel-affinity chromatography as described previously (Bates et al. 2000, 2002; Kaur et al. 2003; Zhong et al. 2007; Ahmed et al. 2010). Proteins were reconstituted into large unilamellar vesicles (LUVs) composed of a 1:1 (molar) mixture of DMPG (1,2-dimyristoyl-*sn*-glycero-3-[phospho-*rac*-(1-glycerol)]) and DMPC (1,2-dimyristoyl-*sn*-glycero-3-phosphocholine) at an initial protein:lipid mass ratio of 1:2, as has been described previously (Ahmed et al. 2010). Further details of the expression, purification, reconstitution, and H/D exchange of MBP are provided in the *Supplementary Information*.

Expression, purification, and reconstitution of Anabaena sensory rhodopsin

Uniformly ^{13}C- and ^{15}N-labeled ASR (UCN ASR) was expressed and purified from *E. coli* cells as has been described previously (Shi et al. 2011). The protein was then reconstituted into liposomes composed of DMPC (1,2-dimyristoyl-*sn*-glycero-3-phosphocholine) and DMPA (1,2-dimyristoyl-*sn*-glycero-3-phosphate) at a 9:1 ratio (w/w), at a protein/lipid ratio of 2:1 (w/w). Further details of the expression, purification, reconstitution, and H/D exchange of ASR are provided in the *Supplementary Information*.

Magic angle spinning solid-state NMR spectroscopy

All NMR experiments on MBP were performed on a Bruker Biospin Avance III spectrometer operating at 600.13 MHz using a Bruker 3.2-mm TL2 ^{1}H–^{13}C–^{15}N

MAS probe. Approximately 4 mg of UCN MBP was center-packed in a 3.2-mm rotor. The effective temperature was kept at 30 °C in all experiments with the spinning frequency set to 10 kHz. All NMR experiments on ASR were performed on a Bruker Biospin Avance III spectrometer operating at 800.230 MHz using a Bruker 3.2-mm TL2 ^{1}H–^{13}C–^{15}N MAS probe. Approximately 4 mg of UCN ASR was center-packed in a 3.2-mm rotor. For consistency with our previous measurements on ASR (Shi et al. 2011; Wang et al. 2011, 2012, 2013a, b), the effective temperature was kept at 5 °C in all experiments, with the spinning frequency set to 14.3 kHz. Sample temperatures were calibrated using an external reference of methanol (Ammann et al. 1982), and were confirmed by the position of the water peak (Hartel et al. 1982).

The pulse sequences used to collect data and additional experimental parameters are provided in Fig. S2 in the *Supplementary Information*. To investigate the sensitivity increase available from proton detection in INEPT-based experiments, we record ^{13}C- and ^{1}H-detected ^{1}H–^{13}C INEPT HSQC spectra on MBP and ASR, collected with the standard pulse sequences shown in Fig. S2c and S2d, respectively (Bodenhausen and Ruben 1980; Bax et al. 1990; Norwood et al. 1990), with acquisition parameters set such that the two experiments take approximately the same amount of time. Two three-dimensional (H)CHH spectra, with proton–proton mixing times of 50 and 150 ms, were collected on both MBP and ASR using the pulse sequence shown in Fig. S2e.

Chemical shifts were referenced to 2,2-dimethyl-2-silapentane-5-sulfonic acid (DSS) using the ^{13}C adamantane downfield peak resonating at 40.48 ppm as a secondary standard (Morcombe and Zilm 2003). One-dimensional spectra and the coherence life time (T_2') (De Paepe et al. 2003) analysis was performed using Topspin 3.1 (Bruker, Karlsruhe, Germany). Two- and three-dimensional spectra were processed with NMRPipe (Delaglio et al. 1995) and a cosine bell squared function was used to apodize the data in all dimensions. The spectra were analyzed in CARA (Keller 2004).

Results and discussion

General characterization of samples by carbon-detected SSNMR

We begin our discussion by describing the one-dimensional SSNMR spectra of MBP and ASR. Magic angle spinning cross-polarization (Pines et al. 1973) (CPMAS) and INEPT (Morris and Freeman 1979; Burum and Ernst 1980) experiments utilize different polarization transfer mechanisms, and thereby allow for the selective excitation of protein regions with differing dynamic characteristics. Whereas CPMAS transfers are based on dipolar couplings and selectively excite rigid regions of the protein, INEPT experiments are based on J-couplings and favor the relatively mobile regions (Andronesi et al. 2005; Etzkorn et al. 2007; Zhong et al. 2007; Stehle et al. 2012).

In the presence of negatively-charged lipids, MBP forms three amphipathic α-helices which anchor the protein onto the membrane, whereas most of the protein remains unstructured and highly flexible (Bates et al. 2003; Zhong et al. 2007; Harauz et al. 2009; Ahmed et al. 2010). In line with this disposition of the protein, Fig. 2a, b shows that INEPT excitation is much more effective than CPMAS on MBP. The linewidths of the peaks observed in the INEPT spectra are much narrower than those in the CPMAS spectra, with J-splitting often being observable in the INEPT spectrum, as shown in the inset. Both spectra were obtained at 30 °C and at a MAS frequency of 10 kHz, and the dependence of MBP spectra on temperature and spinning frequency has been previously investigated (Zhong et al. 2007). We observed a significant decrease in signal intensity at higher MAS frequencies (15–22 kHz), probably due to a reversible water:lipid phase separation and protein dehydration, as has been observed previously in MBP (Zhong et al. 2007). At MAS frequencies of 10 kHz, the molecular motions which facilitate INEPT excitation can be slowed through a decrease in temperature, leading to a decrease in INEPT efficiency and an increase in CPMAS efficiency. However, membrane-bound MBP still exhibits a very high degree of mobility at low temperatures above 0 °C. Below the freezing point of water the CPMAS efficiency is drastically increased, but the spectra become inhomogeneously broadened, indicating that the protein takes on multiple conformations.

In stark contrast to MBP, ASR is a rigid integral α-helical membrane protein with short, often structured, loop regions joining the α-helices. Figure 2c, d compare INEPT and CPMAS spectra collected at a MAS frequency of 14.3 kHz and a temperature of 5 °C, which were chosen so as to be consistent with previous data collected on ASR (Shi et al. 2011; Wang et al. 2011, 2012, 2013a, b). Consistent with the rigidity of the protein, the dipolar-based CPMAS excitation is much more efficient in exciting ASR resonances than INEPT (Fig. 2c, d). Whereas the CPMAS spectrum is very crowded and only very few individual peaks can be resolved, the INEPT spectrum is significantly less populated and several very well-resolved peaks, often with J-splitting evident, are present (Fig. 2c, inset). Although an increase in the sample temperature to 30 °C was found to increase the efficiency of INEPT excitation by approximately two- to eightfold (data not shown), the structure of the INEPT spectrum is largely unchanged, and CPMAS excitation remains significantly more effective.

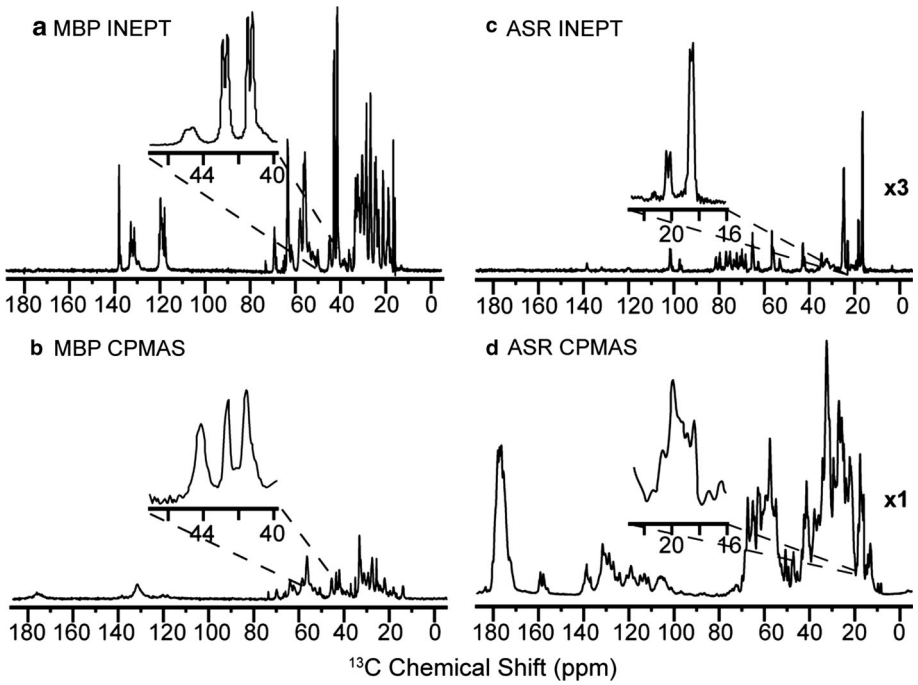

Fig. 2 1D ^{13}C **a** INEPT- and **b** CPMAS-based spectra of UCN MBP. TPPM decoupling of 71.4 kHz was applied during acquisition, the length of which was 25 and 40 ms in the CPMAS and INEPT experiments, respectively. **c** 1D ^{13}C INEPT- and **d** 1D ^{13}C CPMAS-based spectra of UCN ASR. SPINAL64 (Fung et al. 2000) decoupling of ~83 kHz was applied during acquisition, the length of which was 20 and 25 ms in the CPMAS and INEPT experiments, respectively. All spectra were acquired with 2048 scans and are presented without apodization

Furthermore, we found that an increase of the MAS frequency to 20.5 kHz did not significantly improve sensitivity or carbon line widths of the ^{13}C INEPT spectra, implying that the dipolar interactions are sufficiently averaged even at lower magic angle spinning of 14.3 kHz.

The few resonances observed in the ASR ^{13}C INEPT spectrum may originate from amino acids in the mobile regions of the protein, as well as from other mobile species which associate with the protein. Indeed, in addition to several peaks which reside in the aliphatic and sidechain carbon regions (~15–70 ppm), there are several peaks in the 70–80 ppm range which are not present or are below detection in the CPMAS spectrum. Similar peaks have previously been reported in SSNMR spectra of ASR in the *E. coli* membrane (Ward et al. 2015), as well as in the NMR spectra of bacteriorhodopsin (BR) (Patzelt et al. 1997), and of green proteorhodopsin (GPR) (Shi et al. 2009), and have been attributed to carbohydrates that are tightly associated and co-purify with GPR or ASR, or to glycolipids of BR.

We have previously shown that ASR trimer formation occurs in the *E. coli* membrane (Ward et al. 2015). It is possible that the molecules we observe could be trapped between monomers, potentially mediating and contributing to the intermonomer interactions, or be bound in the inner pocket of the trimer. The ASR trimers are stable throughout solubilization and reconstitution (Wang et al. 2012), and, therefore, any molecules which are tightly associated with the trimer in the *E. coli* membrane can be retained in proteoliposomes.

The co-purification of lipids with membrane proteins is a fairly common occurrence, with the majority of observed protein-lipid contacts being due to hydrophobic interactions between the protein and lipid-acyl chains. Indeed, it is not unusual for lipid-acyl chains to be resolvable in crystallographic structures, indicating a high degree of order and rigidity in these regions. For example, the X-ray structure of ASR includes several acyl chains (Vogeley et al. 2004), and the acyl chains seen in the crystal structure of BR (Essen et al. 1998; Belrhali et al. 1999; Luecke et al. 1999) have been well studied and further characterized by neutron diffraction and mass spectrometry (Weik et al. 1998). Although acyl chains are commonly visible in X-ray structures, the remainder of the molecule most often cannot be resolved, implying the presence of significant motions or disorder in these regions. It is possible that lipid molecules bind tightly to ASR through the acyl chains, which are rigid and invisible in the INEPT spectra, whereas the remainder of the molecule remains mobile, and thus is visible in our INEPT spectra. For example, while the acyl chains of the glycolipids are rigid and are visible in the X-ray structure of BR (Essen et al. 1998; Belrhali et al. 1999; Luecke et al.

1999), the headgroups are mobile and are visible in solution-NMR spectra (Patzelt et al. 1997).

The nature of the additional resonances in our ^{13}C INEPT spectrum of ASR has been investigated further by a two-dimensional ^{13}C–^{13}C experiment in which ^{13}C polarization is excited through INEPT, and TOBSY (total through-bond correlation spectroscopy) is utilized to establish correlations between bonded carbon atoms (Fig. 3a black) (Baldus and Meier 1996; Hardy et al. 2001). As both of these methods are based on through-bond transfers, this spectrum differs significantly from that excited using CPMAS and utilizing DARR (dipolar-assisted rotational resonance) for ^{13}C–^{13}C mixing (Fig. 3a red) (Takegoshi et al. 2003; Morcombe et al. 2004). Whereas the INEPT–TOBSY spectrum contains only a few peaks which may correspond to amino acid spin systems, many peaks which are not present in the CPMAS–DARR spectrum are present, particularly in the 70–80 and ~100 ppm ranges. As TOBSY mixing (~7 ms) provides 1–2 bond correlations under our conditions, extended spin systems can be built when multiple cross-peaks are present for a given chemical shift. For example, in Fig. 3b the resonance labeled C5 has cross-peaks with both the C3 and C4 resonances. All three shifts can be assigned to the same spin system if there are also cross-peaks between the C3 and C4 resonances, which is the case in this instance. In Fig. 3b we show that a total of five carbon atoms, which we have numbered based only on their hypothetical order in the molecule, can be incorporated into a single spin system which contains multiple resonances within the 70–80 ppm region, as well as correlations with peaks at ~100 ppm. Thus, this spin system likely represents a carbohydrate moiety (Bradbury and Jenkins 1984), which may be associated with rigid acyl chains that are tightly bound to ASR. In addition to several such spin systems, we also observe spin systems which resemble the headgroups and backbones of phospholipids (Dufourc et al. 2009). Phospholipid headgroups generally contain 2–3 carbon atoms which resonate in the 40–70 ppm range, and cannot always be differentiated from amino acids in this spectrum. The phospholipid backbones (most commonly glycerol, though more complicated alcohols are possible), however, generally consists of three resonances in the 55–75 ppm range (Dufourc et al. 2009), and several such systems can be identified in this spectrum, although these systems could also represent fragments of sugar moieties or lipid headgroups. A full list of assigned spin systems obtained from the two-dimensional ^{13}C–^{13}C INEPT–TOBSY experiment is provided in Table S1.

Water suppression in proton-detected SSNMR spectra

Proton detection in SSNMR is often hindered by the presence of an overpowering water signal which dwarfs all other signals and obscures useful data. In fully-deuterated samples, protons are only present at exchangeable sites, necessitating the incorporation of some percentage of H_2O

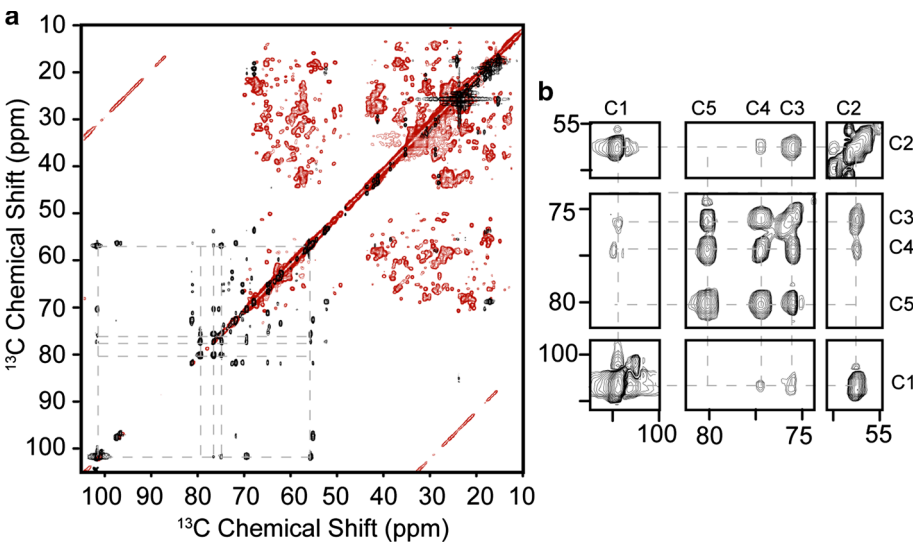

Fig. 3 **a** 2D ^{13}C–^{13}C spectra of UCN ASR obtained with INEPT excitation and TOBSY mixing (*black*) and CPMAS excitation and DARR mixing (*red*). **b** Enlarged regions of the same spectra showing an extended spin system corresponding to a carbohydrate moiety built from the TOBSY correlations available in this spectrum. *Dashed lines* represent spin system connectivities, and the intersections of these lines indicate expected cross-peak positions. As only 1–2 bond correlations are present, not every intersection contains a cross-peak. Many of the spin systems which can be built from the INEPT–TOBSY spectrum are inconsistent with the typical chemical shifts of amino acids, but rather agree with those of carbohydrates and phospholipid headgroups and backbones. Assigned spin systems are summarized in Table S1 in the *Supplementary Information*

in the buffer and the implementation of more complicated water suppression methods (Paulson et al. 2003; Chevelkov et al. 2003; Zhou et al. 2007; Zhou and Rienstra 2008). In contrast, our INEPT-based experiments focus on the detection of non-exchangeable aliphatic protons, and water suppression can be achieved through chemical replacement of the buffer protons with deuterons. This exchange can be achieved by soaking the compacted samples in D_2O buffer. In addition to reducing the strong water signal, this process also results in the replacement of all exchangeable protons in the proteins with deuterons (H/D exchange). Thus, a relatively large volume of D_2O buffer ($\sim$1 mL) is necessary to ensure the exchanged protons, as well as the original H_2O buffer, are sufficiently diluted (at least 100×).

Whereas a large portion of MBP is solvent-accessible and amenable to quick back-exchange, many ASR residues are protected from H/D exchange by the tight packing of α-helices and the membrane environment (Shi et al. 2011; Wang et al. 2011), and studies on a wide range of proteins indicate that such protected regions may experience exchange on a slower time scale (>12 h) (Earnest et al. 1990; Baenziger and Methot 1995; Schulman et al. 1995; Sturgis et al. 1998; Pinheiro et al. 2000; Vinchurkar et al. 2004). In order to ensure complete H/D exchange, our samples were soaked in D_2O buffer for a minimum of 15 h. Fig. S1 shows directly-detected ^{1}H spectra of both MBP and ASR before and after H/D exchange. Although the water is not completely removed in either sample, the drastic reduction of this signal makes two- and three-dimensional proton-detected INEPT-based experiments possible.

Two-dimensional proton-detected SSNMR experiments on myelin basic protein

To investigate the sensitivity enhancement available from proton detection in INEPT-based experiments, we recorded ^{13}C- and ^{1}H-detected ^{1}H–^{13}C INEPT HSQC spectra on MBP, as shown in Figs. 4a, b, respectively. The chemical shifts of the observed cross-peaks in both spectra agree well with assignments which have been made previously on MBP in similar lipid and buffer environments (Zhong et al. 2007), and the type of many peaks can be identified. For example, the peaks located in the carbon $\sim$41–44 ppm and proton $\sim$2.8–3.5 ppm region belong to the CE-HE atoms of lysine residues, or to the CD-HD atoms of arginines. Furthermore, the peaks seen at $\sim$0.8–2 ppm in the proton dimension and $\sim$16–17 ppm in the carbon dimension likely belong to sidechain methyl groups. Although there are many peaks which represent sidechain atoms (carbon shift of $\sim$20–35 ppm), there are noticeably fewer resolved CA resonances (carbon shift of $\sim$45–65 ppm), likely due to the high level of spectral overlap (Zhong et al. 2007). As the mobile regions of MBP which are excited by INEPT are unstructured (Zhong et al. 2007), the chemical shifts are poorly dispersed and many overlapping residues are present, as is characteristic of intrinsically-disordered proteins (Dyson and Wright 2001, 2002). For example, based on previous assignments the peak located at ^{13}C and ^{1}H values of $\sim$69.6 and $\sim$4.0 ppm, respectively, is composed of five overlapping threonine CB/HB peaks, which all have identical proton chemical shifts (within 0.01 ppm) and ^{13}C chemical shifts which vary by only $\sim$0.2 ppm (Zhong et al. 2007).

In the few non-overlapping peaks present in Fig. 4, the average linewidths range from 0.13–0.20 ppm for protons and from 0.35–0.65 ppm for carbons. Coherence life-time, T_2' (De Paepe et al. 2003), measurements indicate values of 4–6 ms for carbons and 5–10 ms for protons. These values correspond to homogeneous proton linewidths of approximately 0.05–0.11 ppm, and carbon linewidths of 0.35–0.55 ppm, which indicates that inhomogeneous broadening, most likely due to conformational heterogeneity which is not completely averaged by fast local molecular motions (Zhong et al. 2007), has only a minimal effect on the linewidths.

As expected, proton detection results in a significant increase in sensitivity, with peaks in the ^{1}H-detected spectrum being $\sim$tenfold more sensitive than those in the ^{13}C-detected spectrum, with values generally ranging from 7 to 12. These values are larger than the increase expected from comparing gamma ratios alone, indicating that other factors, such as the quality factors of the coil, the polarization efficiency, the length of the acquired time domain signal, and the linewidths are responsible for some portion of the enhancement (Ernst et al. 1987; Ishii and Tycko 2000).

Two-dimensional proton-detected SSNMR experiments on *Anabaena* sensory rhodopsin

ASR represents a more challenging case than MBP because both the transmembrane regions and some of the loops are structured and more rigid, experiencing only small amplitude motions, as is evident from the order parameter measurements (Good et al. 2014). To investigate the applicability of proton detection of the mobile fragments, we have compared ^{13}C- and ^{1}H-detected ^{1}H–^{13}C INEPT HSQC spectra of ASR (Figs. 4d, e, respectively). The overall shape of these spectra is very similar to that of MBP, and many cross-peaks are observed in regions which can tentatively be assigned to CA–HA and CB–HB correlations, as well as to the sidechains of lysines and arginines (in the carbon $\sim$41–44 ppm and proton $\sim$2.8–3.5 ppm regions). We also observe many peaks in the $\sim$70–80 ppm region in the carbon dimension, which

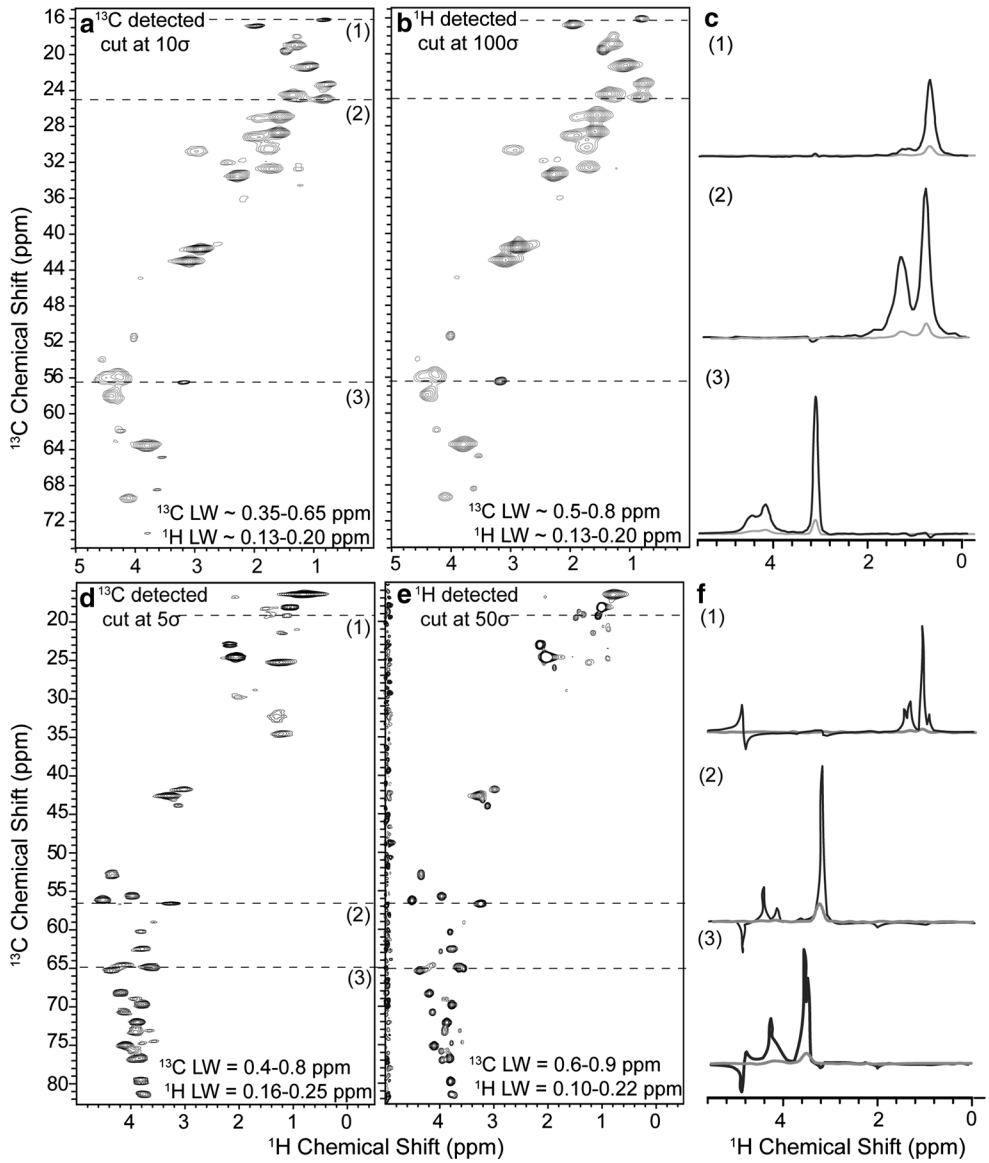

Fig. 4 Comparison of the aliphatic region of the ^{1}H–^{13}C INEPT HSQC spectra of MBP and ASR. **a** ^{13}C-detected and **b** ^{1}H-detected HSQC spectrum of MBP. **d** ^{13}C-detected and **e** ^{1}H-detected HSQC spectrum of ASR. All spectra were collected with a recycle delay of 1.7 s and took approximately 4½ h to acquire. In **c**, **f**, we show 1D traces extracted from the 2D ^{1}H-detected (*black*) and ^{13}C-detected spectra (*grey*) of MBP and ASR, respectively, at the positions indicated by the *dashed lines* and scaled such that the noise amplitudes are equal

we can tentatively assign to the isotopically-labeled lipids or carbohydrates which co-purify with ASR.

Similar to what we have observed in MBP, narrow linewidths are obtained in the directly-detected ^{13}C and ^{1}H dimensions with values ranging from 0.4–0.8 for carbons, and from 0.10–0.22 ppm for protons. The T_2' measurements on ASR reveal values which are generally shorter than those obtained on MBP (3–5 ms in ^{13}C and 3–7 ms in ^{1}H), indicating that once again inhomogeneous broadening does not have a large effect on the linewidths. In line with our observations on MBP, the sensitivity of a given peak is, on average, ~tenfold greater in the ^{1}H-detected spectrum, with values ranging from 7 to 12.

Three-dimensional proton-detected SSNMR experiments on myelin basic protein

The limited resolution of the two-dimensional INEPT-HSQC spectra can be improved by adding the third dimension. In Fig. S2e, we show a pulse sequence for a three-dimensional (H)CHH experiment, which incorporates an additional proton mixing step to facilitate inter-proton

polarization transfer. Active recoupling methods, such as those based on DREAM (Verel et al. 2001), and RFDR (Bennett et al. 1992), were initially tested on MBP and found to be inefficient. Conversely, mixing based on the nuclear Overhauser effect (NOE) (Overhauser 1953; Jeener et al. 1979; Wagner and Wüthrich 1982) was found to result in effective polarization transfer, with the additional benefits of ease of set-up and lack of high-power irradiation, therefore allowing for faster experimental recycling. An additional echo period is added at the end of the pulse sequence to suppress broad proton signals which arise from immobile residues as a result of the final mixing step.

The 3D (H)CHH experiment was performed on MBP with proton mixing times of 50 and 150 ms. Figure 5a shows the two-dimensional ^{13}C–^{1}H projection plane of this experiment acquired with 50 ms of proton–proton mixing and with the t_2 evolution time set to zero [2D (H)C(H)H, spectrum shown in black]. Compared to the two-dimensional ^{1}H–^{13}C INEPT HSQC (shown in blue), additional cross-peaks, resulting from the proton–proton mixing, are seen. The majority of cross-peaks represent intra-residue correlations between neighboring sidechain protons. For example, the CE-HE peaks of lysine and the CD-HD peaks of arginine which were previously identified in the two-dimensional ^{1}H–^{13}C spectra both have cross-peaks at proton shifts of $\sim$1.5–2.0 ppm, which is the expected chemical shift of both HG of arginine and the HD of lysine. In addition to intra-residue correlations, many cross-peaks appear between the amino acid peaks and water, indicating a close association between them. Similar correlations have been observed previously in MBP (Zhong et al. 2007), and are consistent with these amino acids being located either outside of the membrane or in the hydrophilic region of the phospholipid headgroups.

In Fig. 5b, c we show several two-dimensional ^{1}H–^{1}H planes from the (H)CHH experiments. Amino acid systems can be built from data obtained from this spectrum when it is collected with 50 ms of proton mixing by matching proton–proton cross-peaks to obtain the chemical shift values of neighboring carbons. Specifically, cross-peaks provide $C_x[i]$–$H_x[i]$–$H_y[i]$ and $C_y[i]$–$H_y[i]$–$H_x[i]$ correlations (where X, Y = A, B, G, etc.). By matching the

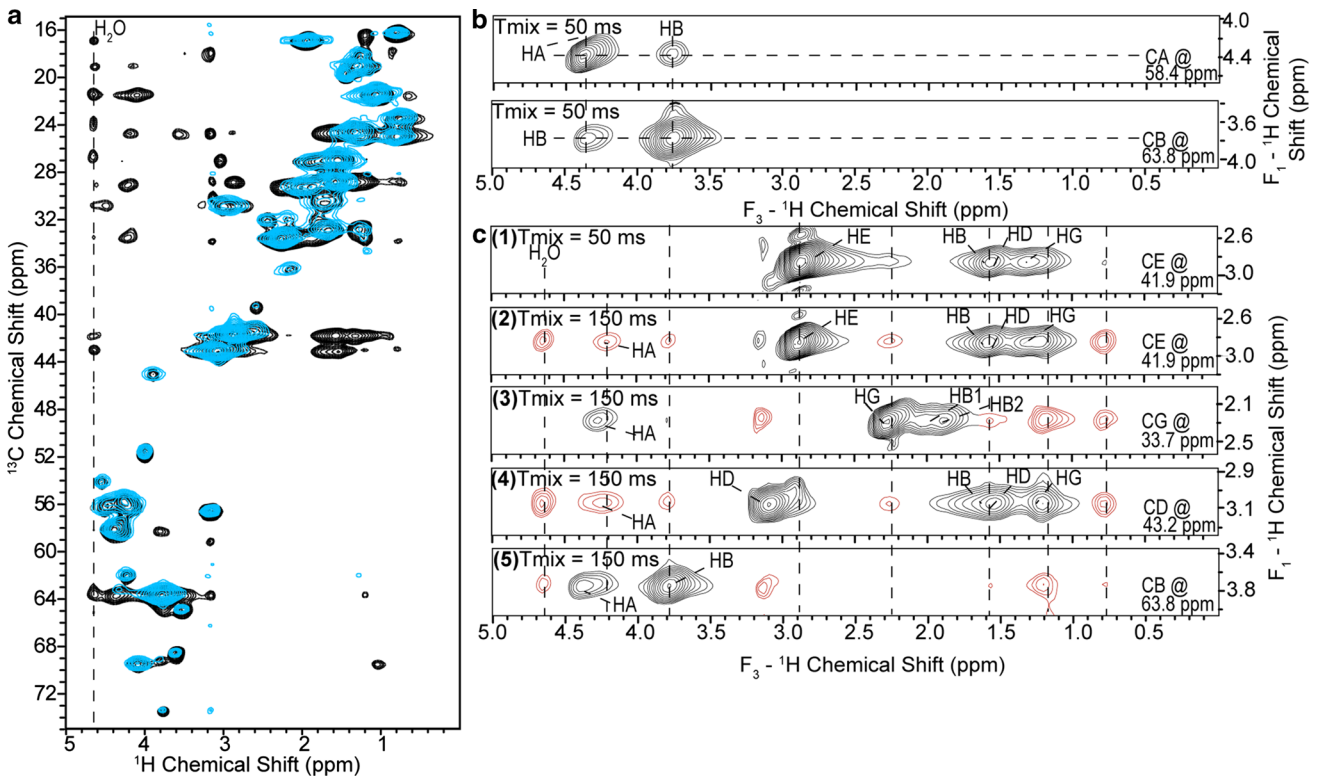

Fig. 5 **a** 2D spectrum of an (H)C(H)H experiment on MBP (*black*) overlaid with the 2D ^{1}H–^{13}C INEPT HSQC (*blue*). Additional cross-peaks which are not present in the 2D ^{1}H–^{13}C INEPT HSQC appear in the 2D (H)C(H)H experiment as a result of the proton–proton mixing (50 ms) and represent intra-residue correlations, as well as correlations between amino acids and water. In **b**, **c**, 2D ^{1}H–^{1}H planes of the 3D (H)CHH experiments are shown. In **b**, we demonstrate how a simple amino acid system can be built by matching cross-peaks in the spectrum collected with 50 ms of proton–proton mixing. In **c**(1), we show that proton information extending HA and HB can be obtained from this experiment by displaying a lysine spin system at the CE ^{13}C position. When the proton–proton mixing period is extended to 150 ms, as shown in panel **c**(2–5), additional cross-peaks (*red*) are observed which correspond to additional intra-residue correlations, as well as inter-residue correlations between protons of neighboring amino acids

H_y–H_x shifts of one system to the H_x–H_y shifts of another, extended C_x[i]–H_x[i]–C_y[i]–H_y[i] systems can be built, as is illustrated in Fig. 5b. Often, several proton–proton cross-peaks are present for a given C_x[i]–H_x[i] pair, as shown in Fig. 5c(1), and the amino acid spin system can be extended by repeating the process described above for multiple H_x[i]–H_y[i] pairs to create complete C_x[i]–H_x[i]–C_y[i]–H_y[i]–C_z[i]–H_z[i]… systems. The amino acid type can then be determined by comparing the chemical shift values to known values for amino acids (Wang and Jardetzky 2002; Ulrich et al. 2008). For example, the C_x[i]–H_x[i]–C_y[i]–H_y[i] system displayed in Fig. 5a can be identified as the CA–HA–CB–HB of a serine residue, and the spin system displayed in Fig. 5b(1) can be identified as a lysine. Using this method, 15 amino acid spin systems can be identified in the three-dimensional (H)CHH experiment. The amino-acid type-specific assignments are summarized in Table S2.

The use of a longer proton mixing period of 150 ms results in additional intra-residue correlations for longer sidechains as well as inter-residue correlations between the amino acids which are spatially close. As can be seen in Fig. 5c(2), such peaks, shown in red, are clearly visible in the spectrum of the lysine spin system acquired with 150 ms mixing time. Peaks such as these can be seen for many other amino acid spin systems in our spectra, and we display several examples in Fig. 5c(3–5). The acquisition of additional intra-residue correlations strengthens and extends amino acid spin system assignments. Inter-residue correlations, which are expected to correspond mostly to sequential correlations due to the unstructured nature of the mobile regions of MBP (Zhong et al. 2007), assist in the assignment process. For example, in Fig. 5c(3) we show two overlapping glutamate systems (as evidenced by the presence of two CB peaks) which are indicated to be spatially close to the lysine shown in Fig. 5c(4), as well as the methyl group of either a leucine, isoleucine, or valine residue. The 18.5-kDa isoform of MBP contains only 8 glutamate residues and, of these, only Q70 is within 1–2 residues of a leucine, isoleucine, or valine residue. Therefore, one of the glutamate systems shown can be tentatively assigned to Q70, and the methyl group to L68. Although a lysine residue also exists in this region (K71), it is not obvious from the data which of the overlapping glutamates is responsible for the correlations seen in Fig. 5c(3).

The identification of additional spin systems in MBP and the acquisition of further sequential assignments are prevented by the large, relative to the spectral dispersion, linewidths obtained in this spectrum and the high degree of spectral overlap, which is characteristic of unstructured proteins. Previously, N and CO assignment data, as well as the combination of several three-dimensional experiments, have been necessary to obtain sequential assignments of MBP (Zhong et al. 2007). The detection of protons will facilitate this process not only through gains in sensitivity, but also through the incorporation of further chemical shift data and an additional dimension in which to resolve systems.

Three-dimensional proton-detected SSNMR experiments on *Anabaena* sensory rhodopsin

To determine the applicability of our three-dimensional proton-detected experiments to ASR, we have also performed the 3D (H)CHH experiment on this sample with proton mixing times of 50 and 150 ms. Fig. S3a shows the two-dimensional ^{13}C–^{1}H projection plane of this experiment acquired with 50 ms of proton–proton mixing and with the t_2 evolution time set to zero [2D (H)C(H)H, spectrum shown in black]. Although many peaks which can be tentatively assigned to amino acid systems are present in the two-dimensional ^{1}H–^{13}C INEPT HSQC spectra (spectrum shown in blue), few proton–proton cross-peaks are observed in these regions in the three-dimensional (H)CHH experiment, even with long proton–proton mixing (150 ms), likely due to the overall rigidity of ASR. However, several more complex systems are observed, which originate from the resonances seen previously in the ^{13}C 70–80 ppm range of the one-dimensional ^{13}C INEPT spectrum, and which have been identified through a 2D ^{13}C–^{13}C INEPT–TOBSY experiment as carbohydrates, as well as lipids. Spin systems which incorporate proton chemical shifts can be built for these molecules in the same manner in which amino acid systems in MBP were created. Fig. S3b shows an example of such a spin system. In addition to the five carbon resonances acquired from the ^{13}C–^{13}C experiment (Fig. 2b), full proton chemical shifts for this spin system have been obtained. Several other such systems could be detected in the 3D (H)CHH spectrum, and a complete list is provided in Table S2. The proton chemical shifts provide additional information for the categorization of these molecules, and allow for the implementation of further proton-detection based experiments which could be used to obtain ^{1}H–^{1}H intermolecular distance restraints, allowing for the determination of binding sites.

Conclusions

Proton detection is an important method for increasing the sensitivity of SSNMR experiments. We have shown here that it can be implemented even at moderate spinning frequencies on a fully-protonated sample to detect mobile entities selectively in membrane proteins. These experiments are demonstrated on two proteins which generally exhibit very different motional regimes. In both cases, narrow lines in both the proton and carbon dimensions are

maintained under direct proton detection. When compared to ^{13}C-detection, we observe an $\sim 10\times$ sensitivity increase in two-dimensional ^{13}C–^{1}H HSQC experiments, and show that these experiments can be easily extended to three dimensions through the incorporation of a proton–proton mixing period.

Through two- and three-dimensional proton-detected experiments performed on MBP, a highly flexible and intrinsically-disordered, peripherally membrane-associated protein, we are able to build amino-acid spin systems which include many sidechain resonances that would not be available on fully-deuterated proteins. In addition, through the incorporation of long proton–proton mixing periods we are able to observe inter-residue correlations which assist in the sequential assignment procedure.

Although our proton-detected experiments on a well-structured and rigid 7TM α-helical protein, ASR, showed fewer intra-protein correlations than were observed in MBP, we were able to observe lipid and carbohydrate resonances. The apparent isotopic labeling of these molecules indicates that they are produced by *E. coli* and co-purify with ASR. Most likely, rigid acyl chains experience strong hydrophobic interactions with the protein, which withstand the solubilization and purification processes. Though the acyl chains which interact with ASR are tightly bound and therefore rigid, the head group regions, which may include bound carbohydrates, remain mobile and therefore are visible in the INEPT-based spectra. These experiments potentially provide a novel method with which to study strong protein-lipid interactions.

Acknowledgments This research was supported by the Natural Sciences and Engineering Research Council of Canada (Discovery Grants to G.H., L.S.B, and V.L.), the Canada Research Chairs Program (G.H.), the Canada Foundation for Innovation, and the Ontario Ministry of Research and Innovation. M.E.W. is supported by the Ontario Graduate Scholarship program. E.R. was a recipient of a Natural Sciences and Engineering Research Council of Canada Postgraduate Fellowship.

References

Agarwal V, Reif B (2008) Residual methyl protonation in perdeuterated proteins for multi-dimensional correlation experiments in MAS solid-state NMR spectroscopy. J Magn Reson 194:16–24

Agarwal V, Diehl A, Skrynnikov N, Reif B (2006) High resolution ^{1}H detected ^{1}H, ^{13}C correlation spectra in MAS solid-state NMR using deuterated proteins with selective ^{1}H, ^{2}H isotopic labeling of methyl groups. J Am Chem Soc 128:12620–12621

Agarwal V, Xue Y, Reif B, Skrynnikov NR (2008) Protein side-chain dynamics as observed by solution- and solid-state NMR spectroscopy: a similarity revealed. J Am Chem Soc 130:16611–16621

Agarwal V, Penzel S, Szekely K, Cadalbert R, Testori E, Oss A, Past J, Samoson A, Ernst M, Böckmann A, Meier BH (2014) De Novo 3D structure determination from sub-milligram protein samples by solid-state 100 kHz MAS NMR spectroscopy. Angew Chem Int Ed 53:12253–12256

Ahmed MAM, Bamm VV, Shi L, Steiner-Mosonyi M, Dawson JF, Brown L, Harauz G, Ladizhansky V (2009) Induced secondary structure and polymorphism in an intrinsically disordered structural linker of the CNS: solid-state NMR and FTIR spectroscopy of myelin basic protein bound to actin. Biophys J 96:180–191

Ahmed MAM, Bamm VV, Harauz G, Ladizhansky V (2010) Solid-state NMR spectroscopy of membrane-associated myelin basic protein–conformation and dynamics of an immunodominant epitope. Biophys J 99:1247–1255

Ahmed MAM, De Avila M, Polverini E, Bessonov K, Bamm VV, Harauz G (2012) Solution nuclear magnetic resonance structure and molecular dynamics simulations of a murine 18.5 kDa myelin basic protein segment (S72-S107) in association with dodecylphosphocholine micelles. Biochemistry 51:7475–7487

Ammann C, Meier P, Merbach AE (1982) A simple multinuclear NMR thermometer. J Magn Reson 46:319–321

Anderson RC, Jarema MA, Shapiro MJ, Stokes JP, Ziliox M (1995) Analytical techniques in combinatorial chemistry: MAS CH correlation in solvent-swollen resin. J Org Chem 60:2650–2651

Andrew ER, Bradbury A, Eades RG (1958) Nuclear magnetic resonance spectra from a crystal rotated at high speed. Nature 182:1659

Andronesi OC, Becker S, Seidel K, Heise H, Young HS, Baldus M (2005) Determination of membrane protein structure and dynamics by magic-angle-spinning solid-state NMR spectroscopy. J Am Chem Soc 127:12965–12974

Asami S, Schmieder P, Reif B (2010) High resolution ^{1}H-detected solid-state NMR spectroscopy of protein aliphatic resonances: access to tertiary structure information. J Am Chem Soc 132:15133–15135

Baenziger JE, Methot N (1995) Fourier transform infrared and hydrogen/deuterium exchange reveal and exchange-resistant core of alpha-helical peptide hydrogens in the nicotinic acetylcholine receptor. J Biol Chem 270:29129–29137

Baldus M, Meier BH (1996) Total correlation spectroscopy in the solid state. The use of scalar couplings to determine the through-bond connectivity. J Magn Reson Ser A 121:65–69

Barbet-Massin E, Pell AJ, Retel JS, Andreas LB, Jaudzems K, Franks WT, Nieuwkoop AJ, Hiller M, Higman V, Guerry P, Bertarello A, Knight MJ, Felletti M, Le Marchand T, Kotelovica S, Akopjana I, Tars K, Stoppini M, Bellotti V, Bolognesi M, Ricagno S, Chou JJ, Griffin RG, Oschkinat H, Lesage A, Emsley L, Herrmann T, Pintacuda G (2014) Rapid proton-detected NMR assignment for proteins with fast magic angle spinning. J Am Chem Soc 136:12489–12497

Bates IR, Matharu P, Ishiyama N, Rochon D, Wood DD, Polverini E, Moscarello MA, Viner NJ, Harauz G (2000) Characterization of a recombinant murine 18.5-kDa myelin basic protein. Protein Expr Purif 20:285–299

Bates IR, Libich DS, Wood DD, Moscarello MA, Harauz G (2002) An Arg/Lys → Gln mutant of recombinant murine myelin basic protein as a mimic of the deiminated form implicated in multiple sclerosis. Protein Expr Purif 25:330–341

Bates IRR, Boggs JMM, Feix JBB, Harauz G (2003) Membrane-anchoring and charge effects in the interaction of myelin basic protein with lipid bilayers studied by site-directed spin labeling. J Biol Chem 278:29041–29047

Bax A, Ikura M, Kay LE, Torchia DA, Tschudin R (1990) Comparison of different modes of 2-dimensional reverse-correlation NMR for the study of proteins. J Magn Reson 86:304–318

Belrhali H, Nollert P, Royant A, Menzel C, Rosenbusch JP, Landau EM, Pebay-Peyroula E (1999) Protein, lipid and water

organization in bacteriorhodopsin crystals: a molecular view of the purple membrane at 1.9 A resolution. Structure 7:909–917

Bennett AE, Griffin RG, Ok JH, Vega S (1992) Chemical shift correlation spectroscopy in rotating solids: radio frequency-driven dipolar recoupling and longitudinal exchange. J Chem Phys 96:8624

Bodenhausen GG, Ruben DJ (1980) Natural abundance nitrogen-15 NMR by enhanced heteronuclear spectroscopy. Chem Phys Lett 69:185–189

Bradbury JH, Jenkins GA (1984) Determination of the structures of trisaccharides by ^{13}C-N.M.R. spectroscopy. Carbohydr Res 126:125–156

Burum DP, Ernst RR (1980) Net polarization transfer via a J-ordered state for signal enhancement of low-sensitivity nuclei. J Magn Reson 39:163–168

Chen L, Kaiser JM, Lai J, Polenova T, Yang J, Rienstra CM, Mueller LJ (2007) J-based 2D homonuclear and heteronuclear correlation in solid-state proteins. Magn Reson Chem 45:S84–S92

Cheng LL, Lean CL, Bogdanova A, Wright SC, Ackerman JL, Brady TJ, Garrido L (1996) Enhanced resolution of proton NMR spectra of malignant lymph nodes using magic-angle spinning. Magn Reson Med 36:653–658

Chevelkov V, van Rossum BJ, Castellani F, Rehbein K, Diehl A, Hohwy M, Steuernagel S, Engelke F, Oschkinat H, Reif B (2003) ^{1}H detection in MAS solid-state NMR spectroscopy of biomacromolecules employing pulsed field gradients for residual solvent suppression. J Am Chem Soc 125:7788–7789

Chevelkov V, Rehbein K, Diehl A, Reif B (2006) Ultrahigh resolution in proton solid-state NMR spectroscopy at high levels of deuteration. Agnew Chem Int Ed 45:3878–3881

Chevelkov V, Habenstein B, Loquet A, Giller K, Becker S, Lange A (2014) Proton-detected MAS NMR experiments based on dipolar transfers for backbone assignment of highly deuterated proteins. J Magn Reson 242:180–188

Dannatt HRW, Taylor GF, Varga K, Higman VA, Pfeil M-P, Asilmovska L, Judge PJ, Watts A (2015) ^{13}C- and ^{1}H-detection under fast MAS for the study of poorly available proteins: application to sub-milligram quantities of a 7 trans-membrane protein. J Biomol NMR 62:17–23

De Avila M, Vassall KA, Smith GST, Bamm VV, Harauz G (2014) The proline-rich region of 18.5 kDa myelin basic protein binds to the SH3-domain of Fyn tyrosine kinase with the aid of an upstream segment to form a dynamic complex in vitro. Biosci Rep 34:775–788

De Paepe G, Giraud N, Lesage A, Hodgkinson P, Bockmann A, Emsley L (2003) Transverse dephasing optimized solid-state NMR spectroscopy. J Am Chem Soc 125:13938–13939

Delaglio F, Grzesiek S, Vuister GW, Zhu G, Pfeifer J, Bax A (1995) NMRPipe—a multidimensional spectral processing system based on Unix pipes. J Biomol NMR 6:277–293

Dufourc EJ, Grelard A, Couvreux A (2009) Lipid signaling protocols: solution and solid-state NMR of lipids. Humana Press, Totowa

Dyson HJ, Wright PE (2001) Nuclear magnetic resonance methods for elucidation of structure and dynamics in disordered states. Methods Enzymol 339:258–270

Dyson HJ, Wright PE (2002) Insights into the structure and dynamics of unfolded proteins from nuclear magnetic resonance. Adv Protein Chem 62:311–340

Earnest TN, Herzfeld J, Rothschild KJ (1990) Polarized Fourier transform infrared spectroscopy of bacteriorhodopsin. Transmembrane alpha helices are resistant to hydrogen/deuterium exchange. Biophys J 58:1539–1546

Ernst RR, Bodenhausen G, Wokaun A (1987) Principles of nuclear magnetic resonance in one and two dimensions. Oxford University Press, Oxford

Essen L, Siegert R, Lehmann WD, Oesterhelt D (1998) Lipid patches in membrane protein oligomers: crystal structure of the bacteriorhodopsin-lipid complex. Proc Natl Acad Sci USA 95:11673–11678

Etzkorn M, Martell S, Andronesi OC, Seidel K, Engelhard M, Baldus M (2007) Secondary structure, dynamics, and topology of a seven-helix receptor in native membranes, studied by solid-state NMR spectroscopy. Angew Chem Int Ed 46:459–462

Fung BM, Khitrin AK, Ermolaev K (2000) An improved broadband decoupling sequence for liquid crystals and solids. J Magn Reson 142:97–101

Gao M, Nadaud PS, Bernier MW, North JA, Hammel PC, Poirier MG, Jaroniec CP (2013) Histone H3 and H4 N-terminal tails in nucleosome arrays at cellular concentrations probed by magic angle spinning NMR spectroscopy. J Am Chem Soc 135:15278–15281

Good DB, Wang S, Ward ME, Struppe J, Brown LS, Lewandowski JR, Ladizhansky V (2014) Conformational dynamics of a seven transmembrane helical protein *Anabaena* sensory rhodopsin probed by solid-state NMR. J Am Chem Soc 136:2833–2842

Goto NK, Kay LE (2000) New developments in isotope labeling strategies for protein solution NMR spectroscopy. Curr Opin Struct Biol 10:585–592

Harauz G, Boggs JM (2013) Myelin management by the 18.5-kDa and 21.5-kDa classic myelin basic protein isoforms. J Neurochem 125:334–361

Harauz G, Libich DS (2009) The classic basic protein of myelin–conserved structural motifs and the dynamic molecular barcode involved in membrane adhesion and protein-protein interactions. Curr Protein Pept Sci 10:196–215

Harauz G, Ladizhansky V, Boggs JM (2009) Structural polymorphism and multifunctionality of myelin basic protein. Biochemistry 48:8094–8104

Hardy EH, Verel R, Meier BH (2001) Fast MAS total through-bond correlation spectroscopy. J Magn Reson 148:459–464

Hartel AJ, Lankhorst PP, Altona C (1982) Thermodynamics of stacking and of self-association of the dinucleoside monophosphate m62A-U from proton NMR chemical shifts: differential concentration temperature profile method. Eur J Biochem 129:343–357

Helmus JJ, Surewicz K, Surewicz WK, Jaroniec CP (2010) Conformational flexibility of Y145Stop human prion protein amyloid fibrils probed by solid-state nuclear magnetic resonance spectroscopy. J Am Chem Soc 132:2393–2403

Hu Y, Doudevski I, Wood D, Moscarello M, Husted C, Genain C, Zasadzinski JAA, Israelachvili J (2004) Synergistic interactions of lipids and myelin basic protein. Proc Natl Acad Sci USA 101:13466–13471

Huber M, Hiller S, Schanda P, Ernst M, Böckmann A, Verel R, Meier BH (2011) A proton-detected 4D solid-state NMR experiment for protein structure determination. ChemPhysChem 12:915–918

Ishii Y, Tycko R (2000) Sensitivity enhancement in solid state (15)N NMR by indirect detection with high-speed magic angle spinning. J Magn Reson 142:199–204

Jeener J, Meier BH, Bachmann P, Ernst R (1979) Investigation of exchange processes by two-dimensional NMR spectroscopy. J Chem Phys 71:4546–4553

Jung KH, Trivedi VD, Spudich JL (2003) Demonstration of a sensory rhodopsin in eubacteria. Mol Microbiol 47:1513–1522

Kaur J, Libich DS, Campagnoni CW, Wood DD, Moscarello MA, Campagnoni AT, Harauz G (2003) Expression and properties of the recombinant murine Golli-myelin basic protein isoform J37. J Neurosci Res 71:777–784

Keifer PA, Baltusis L, Rice DM, Tymiak AA, Shoolery JN (1996) A comparison of NMR spectra obtained for solid-phase-synthesis resins using conventional high-resolution, magic-angle-spinning,

and high-resolution magic-angle-spinning probes. J Magn Reson Ser A 119:65–75

Keller R (2004) The computer aided resonance assignment tutorial, 1st edn. Goldau, Switzerland

Kobayashi T, Mao K, Paluch P, Nowak-Król A, Sniechowska J, Nishiyama Y, Gryko DT, Potrzebowski MJ, Pruski M (2013) Study of intermolecular interactions in the corrole matrix by solid-state NMR under 100 kHz MAS and theoretical calculations. Angew Chem Int Ed Engl 52:14108–14111

Lamley JM, Iuga D, Carl O, Sass H, Rogowski M, Oss A, Past J, Reinhold A, Grzesiek S, Samoson A, Lewandowski R (2014) Solid-state NMR of a protein in a precipitated complex with a full-length antibody. J Am Chem Soc 136:16800–16806

Libich DS, Ahmed MAM, Zhong L, Bamm VV, Ladizhansky V, Harauz G (2010) Fuzzy complexes of myelin basic protein: NMR spectroscopic investigations of a polymorphic organizational linker of the central nervous system. Biochem Cell Biol 88:143–155

Linser R, Dasari M, Hiller M, Higman V, Fink U, Lopez del Amo JM, Markovic S, Handel L, Kessler B, Schmieder P, Oesterhelt D, Oschkinat H, Reif B (2011) Proton-detected solid-state NMR spectroscopy of fibrillar and membrane proteins. Angew Chem Int Ed Engl 50:4508–4512

Lowe IJ (1959) Free induction decays of rotating solids. Phys Rev Lett 2(7):285–287

Luecke H, Schobert B, Richter HT, Cartailler JP, Lanyi JK (1999) Structure of bacteriorhodopsin at 1.55 Å resolution. J Mol Biol 291:899–911

Maas WE, Laukien FH, Cory DG (1996) Gradient, high resolution, magic angle sample spinning NMR. J Am Chem Soc 118:13085–13086

Marchetti A, Jehle S, Felletti M, Knight MJ, Wang Y, Xu Z-Q, Park AY, Otting G, Lesage A, Emsley L, Dixon NE, Pintacuda G (2012) Backbone assignment of fully protonated solid proteins by ^{1}H detection and ultrafast magic-angle-spinning NMR spectroscopy. Angew Chem Int Ed Engl 51:10756–10759

McDermott AE, Creuzet FJ, Kolbert AC, Griffin RG (1992) High-resolution magic-angle-spinning NMR spectra of protons in deuterated solids. J Magn Reson 98:408–413

Mehring M, Pines A, Rhim W-K, Waugh JS (1971) Spin-decoupling in the resolution of chemical shifts in solids by pulsed NMR. J Chem Phys 54:3239–3240

Min Y, Kristiansen K, Boggs JMM, Husted C, Zasadzinski JAA, Israelachvili J (2009) Interaction forces and adhesion of supported myelin lipid bilayers modulated by myelin basic protein. Proc Natl Acad Sci USA 106:3154–3159

Morcombe CR, Zilm KW (2003) Chemical shift referencing in MAS solid state NMR. J Magn Reson 162:479–486

Morcombe CR, Gaponenko V, Byrd RA, Zilm KW (2004) Diluting abundant spins by isotope edited radio frequency field assisted diffusion. J Am Chem Soc 126:7196–7197

Morris G, Freeman R (1979) Enhancement of nuclear magnetic resonance signals by polarization transfer. J Am Chem Soc 233:760–762

Mulder FAA, Hon B, Muhandiram DR, Dahlquist FW, Kay LE (2000) Flexibility and ligand exchange in a buried cavity mutant of T4 lysozyme studied by multinuclear NMR. Biochemistry 39:12614–12622

Nishiyama Y, Zhang R, Ramamoorthy A (2014) Finite-pulse radio frequency driven recoupling with phase cycling for 2D (1)H/(1)H correlation at ultrafast MAS frequencies. J Magn Reson 243:25–32

Norwood TJ, Boyd J, Heritage JE, Soffe N, Campbell ID (1990) Comparison of techniques for ^{1}H-detected heteronuclear ^{1}H–^{15}N spectroscopy. J Magn Reson 87:488–501

Overhauser AW (1953) Polarization of nuclei in metals. Phys Rev 92:411–415

Parthasarathy S, Nishiyama Y, Ishii Y (2013) Sensitivity and resolution enhanced solid-state NMR for paramagnetic systems and biomolecules under very fast magic angle spinning. Acc Chem Res 46:2127–2135

Patzelt H, Ulrich AS, Egbringhoff H, Düx P, Ashurst J, Simon B, Oschkinat H, Oesterhelt D (1997) Towards structural investigations on isotope labelled native bacteriorhodopsin in detergent micelles by solution-state NMR spectroscopy. J Biomol NMR 10:95–106

Paulson EK, Morcombe CR, Gaponenko V, Dancheck B, Byrd RA, Zilm KW (2003) Sensitive high resolution inverse detection NMR spectroscopy of proteins in the solid state. J Am Chem Soc 125:15831–15836

Pines A, Gibby MG, Waugh JS (1973) Proton-enhanced NMR of dilute spins in solids. J Chem Phys 59:569–590

Pinheiro TJT, Cheng H, Seeholzer SH, Roder H (2000) Direct evidence for the cooperative unfolding of cytochrome c in lipids membranes from ^{1}H–^{1}H exchange kinetics. J Mol Biol 303:617–626

Polverini E, Rangaraj G, Libich DS, Boggs JM, Harauz G (2008) Binding of the proline-rich segment of myelin basic protein to SH3 domains: spectroscopic, microarray, and modeling studies of ligand conformation and effects of posttranslational modifications. Biochemistry 47:267–282

Reif B, Jaroniec CP, Rienstra CM, Hohwy M, Griffin RG (2001) ^{1}H–^{1}H MAS correlation spectroscopy and distance measurements in a deuterated peptide. J Magn Reson 151:320–327

Reif B, Xue Y, Agarwal V, Pavlova MS, Hologne M, Diehl A, Ryabov YE, Skrynnikov NR (2006) Protein side-chain dynamics observed by solution- and solid-state NMR: comparative analysis of methyl ^{2}H relaxation data. J Am Chem Soc 128:12354–12355

Schulman BA, Redfiend C, Peng Z, Dobson CM, Kim PS (1995) Different Subdomains are most protected from hydrogen exchange in the molten globule and native states of human [alpha]-lactalbumin. J Mol Biol 253:651–657

Shi L, Ahmed MAM, Zhang W, Whited G, Brown LS, Ladizhansky V (2009) Three-dimensional solid-state NMR study of a seven-helical integral membrane proton pump–structural insights. J Mol Biol 386:1078–1093

Shi L, Kawamura I, Jung K-H, Brown LS, Ladizhansky V (2011) Conformation of a seven-helical transmembrane photosensor in the lipid environment. Angew Chem Int Ed 50:1302–1305

Stehle J, Scholz F, Löhr F, Reckel S, Roos C, Blum M, Braun M, Glaubitz C, Dötsch V, Wachtveitl J, Schwalbe H (2012) Characterization of the ground state dynamics of proteorhodopsin by NMR and optical spectroscopies. J Biomol NMR 54:401–413

Sturgis J, Robert B, Goormaghtigh E (1998) Transmembane helix stability: the effect of helix-helix interactions studied by Fourier transform infrared spectroscopy. Biophys J 74:988–994

Takegoshi K, Nakamura S, Terao T (2003) ^{13}C–^{1}H dipolar-driven ^{13}C–^{13}C recoupling without ^{13}C rf irradiation in nuclear magnetic resonance of rotating solids. J Chem Phys 118:2325–2341

Tian Y, Chen L, Niks D, Kaiser JM, Lai J, Rienstra CM, Dunn MF, Mueller LJ (2009) J-Based 3D sidechain correlation in solid-state proteins. Phys Chem Chem Phys 11:7078–7086

Ulrich EL, Akutsu H, Doreleigers JF, Harano Y, Ioannidis YE, Lin J, Livny M, Mading S, Mazuik D, Miller Z, Nakatani E, Schulte CF, Tolmie DE, Wenger RK, Yao H, Markley JL (2008) BioMagResBank. Nucliec Acids Res 36:D402–D408

Van Melckebeke H, Schanda P, Gath J, Wasmer C, Verel R, Lange A, Meier BH, Bockmann A (2011) Probing water accessibility in

HET-s(218-289) amyloid fibrils by solid-state NMR. J Mol Biol 405:765–772

Verel R, Ernst M, Meier BH (2001) Adiabatic dipolar recoupling in solid-state NMR: the DREAM scheme. J Magn Reson 150:81–99

Vinchurkar MS, Chen KHC, Yu SSF, Kuo SJ, Chiu HC, Chien SH, Chan SI (2004) Polarized ATR-FTIR spectroscopy of the membrane-embedded domains of the particulate methane monooxygenase. Biochemistry 43:13283–13292

Vogeley L, Sineshchekov OA, Trivedi VD, Sasaki J, Spudich JL, Luecke H (2004) *Anabaena* sensory rhodopsin: a photochromic color sensor at 2.0 A. Science 306:1390–1393

Wagner G, Wüthrich K (1982) Sequential resonance assignments in protein ^{1}H nuclear magnetic resonance spectra. J Mol Biol 155:347–366

Wang Y, Jardetzky O (2002) Probability-based protein secondary structure identification using combined NMR chemical-shift data. Protein Sci 11:852–861

Wang S, Shi L, Kawamura I, Brown LS, Ladizhansky V (2011) Site-specific solid-state NMR detection of hydrogen-deuterium exchange reveals conformational changes in a 7-helical transmembrane protein. Biophys J 101:L23–L25

Wang S, Munro R, Kim S, Jung K-H, Brown LS, Ladizhansky V (2012) Paramagnetic relaxation enhancement reveals oligomerization interface of a membrane protein. J Am Chem Soc 134:16995–16998

Wang S, Munro RA, Shi L, Kawamura I, Okitsu T, Wada A, Kim S-Y, Jung K-H, Brown LS, Ladizhansky V (2013a) Solid-state NMR spectroscopy structure determination of a lipid-embedded heptahelical membrane protein. Nat Methods 10:1007–1015

Wang S, Shi L, Okitsu T, Wada A, Brown LS, Ladizhansky V (2013b) Solid-state NMR ^{13}C and ^{15}N resonance assignments of a seven-transmembrane helical protein *Anabaena* sensory rhodopsin. Biomol NMR Assign 7:253–256

Ward ME, Shi L, Lake EM, Krishnamurthy S, Hutchins H, Brown LS, Ladizhansky V (2011) Proton-detected solid-state NMR reveals intramembrane polar networks in a seven-helical transmembrane protein proteorhodopsin. J Am Chem Soc 133:17434–17443

Ward ME, Wang S, Munro R, Ritz E, Hung I, Gorkov PL, Jiang Y, Liang H, Brown LS, Ladizhansky V (2015) In situ structural studies of *Anabaena* sensory rhodopsin in the *E. coli* inner membrane. Biophys J 108:1683–1696

Weik M, Patzelt H, Zaccai G, Oesterhelt D (1998) Localization of glycolipids in membranes by in vivo labeling and neutron diffraction. Mol Cell 1:411–419

Weingarth M, Van Der Cruijsen EAW, Ostmeyer J, Lievestro S, Roux B, Baldus M (2014) Quantitative analysis of the water occupancy around the selectivity filter of a K^{+} channel in different gating modes. J Am Chem Soc 136:2000–2007

Weininger U, Blissing AT, Hennig J, Ahlner A, Liu Z, Vogel HJ, Akke M, Lundström P (2013) Protein conformational exchange measured by ^{1}H R1ρ relaxation dispersion of methyl groups. J Biomol NMR 57:47–55

Yang J, Aslimovska L, Glaubitz C (2011) Molecular dynamics of proteorhodopsin in lipid bilayers by solid-state NMR. J Am Chem Soc 133:4874–4881

Ye YQ, Malon M, Martineau C, Taulelle F, Nishiyama Y (2014) Rapid measurement of multidimensional ^{1}H solid-state NMR spectra at ultra-fast MAS frequencies. J Magn Reson 239:75–80

Zhong L, Bamm VV, Ahmed MAM, Harauz G, Ladizhansky V (2007) Solid-state NMR spectroscopy of 18.5 kDa myelin basic protein reconstituted with lipid vesicles: spectroscopic characterisation and spectral assignments of solvent-exposed protein fragments. Biochim Biophys Acta 1768:3193–3205

Zhou DH, Rienstra CM (2008) High-performance solvent suppression for proton detected solid-state NMR. J Magn Reson 192:167–172

Zhou DH, Shah G, Cormos M, Mullen C, Sandoz D, Rienstra CM (2007) Proton-detected solid-state NMR spectroscopy of fully protonated proteins at 40 kHz magic-angle spinning. J Am Chem Soc 129:11791–11801